Nano Energy 109 (2023) 108299

Contents lists available at ScienceDirect

Nano Energy

journal homepage: www.elsevier.com/locate/nanoen

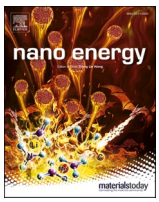

Customizable self-powered pressure sensor based on piezo-transmittance of tilted structures

Lei Wu [a,b], Junseong Ahn [b], Jungrak Choi [b], Jimin Gu [b], Xuan Li [b], Osman Gul [b], Zhi-Jun Zhao [c], Linmao Qian [a], Bingjun Yu [a,*], Inkyu Park [b,*]

[a] Tribology Research Institute, State Key Laboratory of Traction Power, Southwest Jiaotong University, Chengdu 610031, China
[b] Department of Mechanical Engineering, Korea Advanced Institute of Science and Technology (KAIST), Daejeon 34141, Republic of Korea
[c] Institute of Smart City and Intelligent Transportation, Southwest Jiaotong University, Chengdu 611756, China

ARTICLE INFO

Keywords:
Self-powered sensor
Pressure sensor
Piezo-transmittance
Tilted structures
Customizable sensor

ABSTRACT

In the era of the Internet of Things, there is an increasing demand for specialized self-powered sensors owing to extensive applications involving an enormous number of distributed devices in numerous fields. However, realizing self-powered sensors with excellent predictability and designability to accommodate diverse application requirements remains a significant challenge because of the randomness of the nanomaterials or micro/nano-porous structures used. This report describes the development of a customizable and designable self-powered pressure sensor based on the piezo-transmittance of opaque tilted structures. The light transmittance decreases with increasing pressure owing to the deformation of tilted structures. Piezo-transmittance sensors with various linear ranges were customized by rationally designing Young's moduli and structural parameters and optimizing cross-sectional architectures of tilted structures. The pressure sensor was fabricated by molding on 3D-printed master patterns comprising various tilted structures. Each customized sensor exhibits excellent static and dynamic responses, and responses are unaffected by light intensity, ambient temperature, and humidity. Finally, the piezo-transmittance sensors were applied to a self-powered wireless breath monitoring system that integrated flexible solar cell and Bluetooth Low Energy, an all-weather wind detection system with simultaneous signal processing and energy harvesting, and a real-time control system for teleoperated a robotic manipulation.

1. Introduction

With the rapid development of the Internet of Things (IoT), diverse smart electronic devices, such as wearable sensors, implantable devices, and smart windows, have been extensively applied in healthcare and environmental monitoring to improve the quality and safety of human's life [1–5]. Reports have predicted that the number of these smart devices will reach approximately 125 billion by 2030 [6]. However, providing sustainable and convenient power for such an enormous number of distributed devices remains a significant challenge in the IoT era [7]. In this regard, self-powered sensing systems utilizing clean energy including solar power or mechanical motions have emerged as attractive solutions [8]. These sensing systems have the advantages that they do not require frequent charging and replacement of their power supplies, and this is beneficial when the devices are installed in the places that are remote or difficult to access [9,10]. Among the most essential sensing elements in the IoT systems, pressure sensors have attracted unprecedented interest because of their applications in human-machine interaction, health diagnosis, and electronic skin [11–15]. Various sensing mechanisms including piezoelectric, piezocapacitive, piezoresistive, and triboelectric methods have been applied to convert pressure stimuli to electrical signals [16–18]. In general, piezoresistive and piezocapacitive sensor need to have an extra power supply, which inevitably require frequent charging and regular replacement, making them unsuitable for remote and long-term monitoring [19]. Piezoelectric and triboelectric devices present excellent abilities to monitor dynamic pressures without requiring an extra power supply, but they cannot detect static pressures owing to the impulsive output signals [20]. Therefore, utilizing common sensing mechanisms to realize self-powered pressure sensor for continuous detection of dynamic and static pressures remains a huge challenge.

Recently, owing to their rapid response, high sensitivity, and long-

* Corresponding authors.
E-mail addresses: bingjun@swjtu.edu.cn (B. Yu), inkyu@kaist.ac.kr (I. Park).

https://doi.org/10.1016/j.nanoen.2023.108299
Received 16 December 2022; Received in revised form 30 January 2023; Accepted 19 February 2023

term stability, piezo-transmittance sensors based on the change in light intensity have garnered increasing attention [21,22]. More critically, such sensors enable the detection of static and dynamic pressures without extra power supply. Choi et al. [23] proposed a self-powered piezo-transmittance sensor comprising a microporous elastomer and flexible solar cell. In this device, with an increasing pressure, the closure of the micropores results in less light scattering and higher light transmittance. Wang et al. [24] proposed mechanically responsive smart windows offering the advantages of rapid response and excellent repeatability by utilizing hydrogen bonding and surface roughness compensation between hydrogel and agar films. However, their piezo-transmittance responses can be hardly predicted and designed due to random distribution of micropores or rough surfaces, resulting in poor reproducibility and accuracy for pressure sensing.

Notably, the performance requirements of sensing systems can differ considerably depending on the applications [25]. Developing novel material and structural design in tandem with fabrication strategies could provide a means of fulfilling the requirement for different application scenarios [4,26]. However, the development of different materials and structures depending on the applications is time-consuming and labor-intensive [27]. As an alternative way, pressure sensors with customizable sensitivities and linear pressure ranges can achieve more accurate and efficient pressure sensing [28–30]. Therefore, it is highly desirable to develop self-powered piezo-transmittance sensors with excellent predictability and designability for accommodating diverse application requirements.

Herein, we developed a self-powered pressure sensor with excellent predictability and designability based on the piezo-transmittance of opaque tilted structures (including tilted pillars and walls). For proposed self-powered pressure sensor consisting of solar cells and piezo-transmittance structures, the light transmittance change under condition of both constant and pulse stimuli can be detected by measuring the output electrical signals of solar cells without external power [31]. This can be attributed to the stable output current characteristics without any

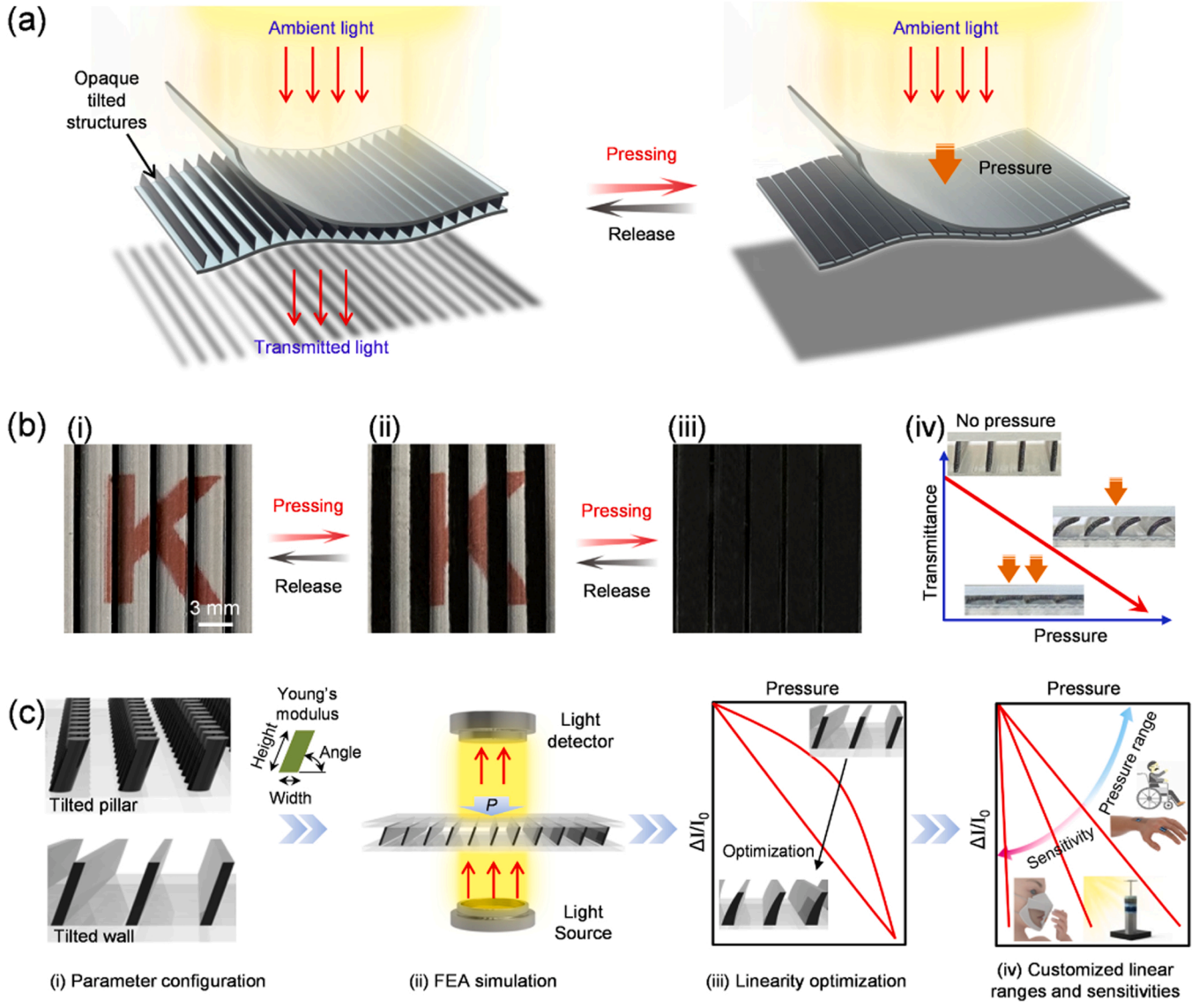

Fig. 1. Principle, light transmittance change, and customization process of proposed self-powered pressure sensor. (a) Schematic diagram depicting the sensor structure and working principle of the pressure sensor. (b) (i-iii) Top views of the tilted structures and (iv)the variations in light transmittance with an increase in the pressure. The insets display cross section view of tilted structures with the increasing pressure. (c) Customization process for piezo-transmittance sensors with various linear pressure ranges and sensitivities. (i) Rationally designing structural parameters (tilted angle, width, and height) and Young's modulus of tilted structures. (ii) FEA simulation for the light transmittance response of constructed pressure sensor. (iii) Linearity enhancement by optimizing the cross-sectional profiles of tilted structures. (iv) Realization of piezo-transmittance sensors with various linear pressure ranges and sensitivities to accommodate diverse application requirements.

short-term output decay. Therefore, the proposed self-powered pressure sensors can simultaneously detect both static and dynamic pressures. A finite element analysis (FEA) simulation was performed to predict and optimize light transmittance change of these pressure sensors comprising various tilted structures. By rationally designing Young's moduli and structural parameters, and optimizing the cross-sectional architectures of tilted structures, piezo-transmittance sensors with linear pressure ranges of 1 (L-sensor), 10 (M-sensor), and 65 kPa (H-sensor) were realized. Dynamic and static responses for each customized pressure sensor were further investigated. The L-sensor sensor was successfully utilized in a self-powered wireless breath monitoring system that integrated flexible solar cell and Bluetooth low energy (BLE). The M-sensor was applied to an all-weather wind detection system with simultaneous signal processing and energy harvesting. In addition, the application of H-sensor in real-time teleoperated control system for robotic grasping was demonstrated.

2. Results and discussion

2.1. Working principle and customizable process

Fig. 1a illustrates a schematic of the proposed piezo-transmittance sensor featuring with a sandwich structure composed of opaque tilted structures, and top and bottom transparent elastomer substrates. The piezo-transmittance sensor was fabricated by molding on fused deposition modeling (FDM) 3D-printed master patterns comprising various opaque tilted structures (Fig. S1 in the Supplementary Material), and the detailed information is presented at Experimental Section. Accordingly, the scale of tilted structures is limited by the resolution of 3D printer. In this paper, the minimum scale of single tilted structure (height and width) is 500 μm, which can determine the minimum scale of a tilted structure to work as a pressure sensor. The maximum scale of a tilted structure to work as a pressure sensor should be determined by practical application requirements. Under an ambient light environment, light transmittance decreases with increasing pressure because of the deformation of opaque tilted structures. Fig. 1b presents top views of the tilted structures and the variations in light transmittance with an increase in the pressure. As can be seen, the decrease in light transmittance with the increasing pressure results in the gradual disappearance of the letter "K" in the background.

Because of the increasing demand for specialized self-powered sensors in IoTs era, it has become necessary to develop a designable and predictable sensor. Fig. 1c displays the customization process of the proposed piezo-transmittance sensor. First, the structure type (including tilted pillars and tilted walls), structural parameters, namely, tilted angle, width, and height; and Young's moduli are rationally designed. Elastomer substrates including polydimethylsiloxane (PDMS) and Ecoflex are typical hyperelastic materials, and their Young's moduli increase with higher deformation in a nonlinear fashion [32]. Moreover, the tilted structures not only undergo compression deformation under the applied pressure, but also withstand toppling and bending deformation [33]. In view of this, it is difficult to use theoretical models to predict the light transmittance change of pressure sensors. To this end, variations in the light transmittance change of constructed pressure sensor are predicted by performing a FEA simulation (Details regarding the FEA simulation model are provided in Experimental Section), where elastomer substrates and tilted structures were set as the Mooney–Rivlin model with hyperelastic properties [34], thereby obtaining pressure-sensing response including sensitivity, sensing range, and linearity. The simulation results were compared with data generated by experimental characterization to further confirm the validity. Next, based on the simulation and experiment results, the data fitting and/or machine learning were introduced to further determine design law of the pressure sensors, thereby realizing inversely designed sensor parameters for the customization process (Fig. S2). Furthermore, the linearity is significantly enhanced by designing the cross-sectional architectures of tilted structures from ones with constant widths to arc shapes with continuous width gradients (The details can be found in the next Section). With regard to specific applications, the trade-off between the sensitivity and pressure range is crucial for preserving high monitoring accuracy and effectiveness. For instance, the respiration and light breeze often generates a subtle pressure (<1 kPa); gentle touches and strong wind can cause a pressure of over 1 kPa; a relatively high pressure (>10 kPa) is produced during dramatic human movements [23]. Finally, the piezo-transmittance sensors with various linear pressure ranges and sensitivities are customized by designing the opaque tilted structures to accommodate diverse application requirements.

2.2. Simulation and characterization for piezo-transmittance sensor

The responses of the piezo-transmittance sensors were simulated and characterized to further demonstrate their predictability and designability. The FEA simulation model comprised two modules, namely, solid mechanics and geometrical optics modules. Fig. 2a displays the simulation results for a piezo-transmittance sensor comprising tilted walls under a pressure of 10 kPa, and the cross-sectional view of mechanical simulation results and top view of optical simulation results under pressures of 10 and 40 kPa are shown in Fig. 2b and c, respectively. The amounts of transmitted light under different pressure were calculated based on the yellow area shown in the optical simulation results. The relative light transmittance change is defined as $\Delta I/I_0$, where I_0 and ΔI represent the initial light intensity and light transmittance change under the applied pressure, respectively. Fig. 2d presents a comparison between the simulation and experimental results for the response of the piezo-transmittance sensor composed respectively of tilted pillars and tilted walls featuring identical width (750 μm), height (2 mm), tilted angle (70°) and Young's modulus (1.5 MPa, which is the value for PDMS with a 10:1 mass ratio of base to cross-linker) [35]. Excellent consistency between simulation and experiment results was evident, demonstrating a remarkable predictability for the proposed piezo-transmittance sensors. Notably, the piezo-transmittance sensor comprising tilted walls presents higher pressure range (65 kPa), and the light is completely blocked under high pressure because the minimum value of $\Delta I/I_0$ can reach −1. By comparison, the piezo-transmittance sensor comprising tilted pillars presents a lower pressure range (16 kPa), and its detection limit (3 Pa) is much less than that of the piezo-transmittance sensor comprising tilted walls (25 Pa) (Fig. S3), rendering it more suitable for detecting low pressures with the same structural parameters. However, it should be noted that gaps exist between adjacent tilted pillars, resulting in an incomplete blockage for the light under relatively high pressure and thereby leading to a limited sensitivity. Therefore, even though piezo-transmittance sensors comprising tilted pillars have lower detection limit and pressure range, its sensitivity (0.02 kPa^{-1}) is not much higher than the piezo-transmittance sensor comprising tilted walls (0.015 kPa^{-1}). Furthermore, the influence of structure size (i.e., whether it was on the order of micrometers or millimeters) on the light transmittance change was simulated, and the results are displayed in Fig. S4. The sensors with sizes the on order of micrometers or millimeters exhibit same light transmittance change, demonstrating that proportionally scaling the structure size down or up does not change the sensor response. Therefore, the scale of the proposed pressure sensor can be reduced using 3D printer with higher resolution without affecting the sensor performance.

Effects of structural parameters and Young's moduli of tilted structures on the variations in light transmittance were further investigated using pressure sensors comprising tilted walls, and the corresponding results are presented in Fig. 2e–h. It is evident that the sensor responses are considerably affected by the structural parameters (including tilted angle, width, and height), and Young's modulus. As the angle of tilted structures (width= 750 μm, height= 2 mm, and Young's modulus= 1500 kPa) increased from 40° to 80° (The cross-sectional topographies are shown in Fig. S5), the pressure range of fabricated sensors gradually

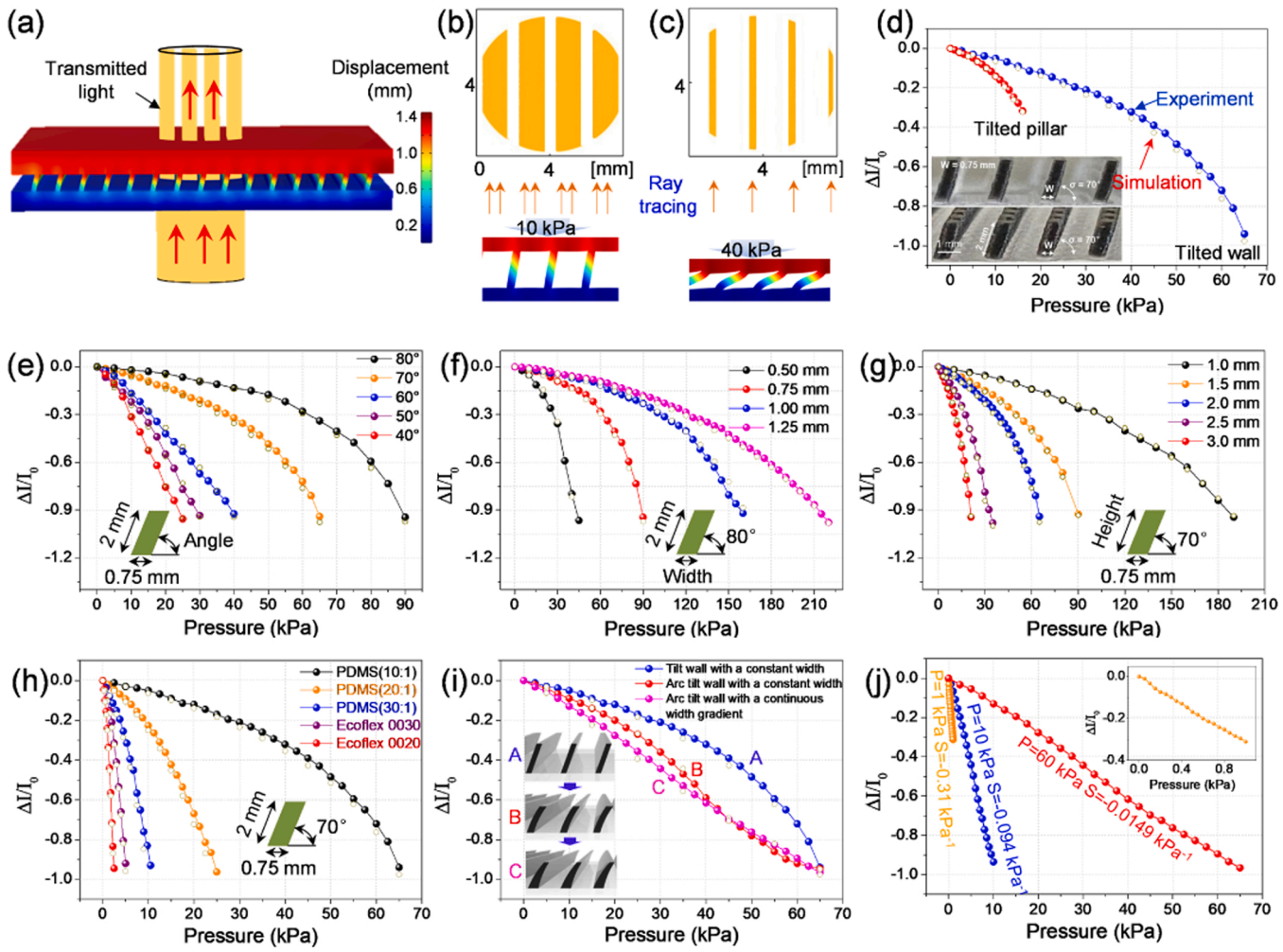

Fig. 2. FEA simulation and experimental characterizations for the piezo-transmittance sensor with different parameters to customize linear pressure ranges and sensitivities. (a) The simulation results for tilted wall (height= 2 mm, width= 0.5 mm, tilted angle= 80°, and Young's modulus = 1500 kPa) under a pressure of 10 kPa. The color refers to the displacement in vertical direction. (b) Cross-sectional view of mechanical simulation results and (c) top view of optical simulation results under 10 and 40 kPa. Yellow areas correspond to the transmitted light. (d) Comparison of simulation and experiment results for light transmittance change of sensors comprising tilted pillar and wall. The insets show the cross-sectional topographies. (e)–(h) Effects of tilted angle (40°, 50°, 60°, 70°, and 80°; width= 0.75 mm, height= 2 mm), width (0.5, 0.75, 1.0, and 1.25 mm; tilted angle= 80°, height= 2 mm), height (1.0, 1.5, 2.0, 2.5, and 3.0 mm; tilted angle= 70°, width= 0.75 mm), and Young's modulus (60, 125, 245, 600, and 1500 kPa) of tilted structures on the relative light transmittance change of the pressure sensor. (i) Impact of structure architecture (tilted wall with constant width, arc tilted wall with constant width, and arc tilted wall with a continuous width gradient) on the piezo-transmittance properties. (j) Realization of linear pressure range of 1, 10, and 65 kPa.

increased from 25 to 90 kPa (Fig. 2e). With the increasing width from 500 μm to 1.25 mm (Fig. S6), the pressure range rose from 45 to 220 kPa (Fig. 2f). Fig. 2g plots the relative light transmittance change of pressure sensor comprising tilted wall with different heights (1.0, 1.5, 2.0, 2.5, and 3.0 mm) and same width (750 μm), tilted angle (70°) and Young's modulus (1500 kPa) (Fig. S7). The pressure range decreased with the increase of the height of the tilted structures. Remarkably, the pressure range of the piezo-transmittance sensors with same structural parameters exhibited a positive correlation with the Young's modulus of tilted structures (Fig. 2h). The Young's moduli for different elastomers are listed in Table S1. Consequently, piezo-transmittance sensors with suitable pressure ranges and sensitivities according to different application scenarios can be customized by rationally designing these geometrical and material parameters.

For practical pressure sensor applications, high linearity enables pressure-response calibration process to be bypassed, thereby simplifying the data processing system and improving response speed of sensing system [36]. However, the piezo-transmittance sensor comprising either tilted pillars or tilted walls presented poor linearity at high pressure (Fig. 2d–h), and thus linearity enhancement was essential. Fig. S8 further analyzes the typical mechanical simulation results for a piezo-transmittance sensor with pressure range of 65 kPa. The results show that the deformation of tilted structures with constant widths goes through two stages. Specifically, toppling deformation dominated at relative low pressure (0–30 kPa), whereas both toppling and bending deformation occurred at high pressure (30–65 kPa). Such results indicate that poor linearity of piezo-transmittance sensor could be ascribed to the deformation difference between low and high applied pressure. Accordingly, optimizing the cross-sectional architectures of tilted structures could significantly enhance the linearity. Considering that arc tilted structures undergo both toppling and bending deformations not only at low pressures but also at high pressures (Fig. S9a), the cross-sectional profiles of tilted structures were optimized from ones with constant widths to arc shapes with constant width. Fig. 2i further displays the simulation and experiment results for the light transmittance change of these two types of structures. The linearity of the piezo-transmittance sensor comprising arc tilted walls was enhanced to some extent but it remained unsatisfactory. It is also noted that

increasing the sensitivity at low pressure and decreasing the sensitivity at high pressure could yield a piezo-transmittance sensor with wide linear pressure range. To this end, the response of piezo-transmittance sensor comprising arc-tilted walls with a continuous width gradient (Fig. S10) was further simulated and characterized. The results demonstrated a good linearity within a pressure range of 65 kPa (Fig. 2i). By rationally designing structural parameters and predicting the response using FEA simulation, the linear pressure range of 10 kPa and 1 kPa was also realized (Fig. 2j). The topographies of these structures are shown in Fig. S11. These results demonstrated that the proposed piezo-transmittance sensors possessed an excellent designability and customizability.

2.3. Sensing performance

The static and dynamic response performances of piezo-transmittance sensors with linear pressure range of 65 kPa (H-sensor), 10 kPa (M-sensor), and 1 kPa (L-sensor) were investigated at a light intensity of 200 W/m^2. The change in light transmittance ($\Delta I/I_0$) for these three sensors under a wide range of representative pressures (H-sensor: 5, 20, 35, 45, and 65 kPa; M-sensor: 0.5, 1.0, 3.5, 5.0, and 10 kPa; L-sensor: 0.05, 0.1, 0.3, 0.5, and 1.0 kPa) were studied, and the results are presented in Fig. 3a–c. It was demonstrated that each piezo-transmittance sensor exhibited a stable and repeatable response. Fig. 3d further showed a fast response time of 60 ms and a rapid recovery time of 42 ms for H-sensor, which were calculated within the 10–90 % of light transmittance response to the applied pressure. Moreover, the rapid response and recovery were also detected from M-sensor and L-senor, as displayed in Figs. S12a and S13a. The loading and unloading curves demonstrated a reversible response and low hysteresis (within 8 %) [37], as shown in Fig. 3e, S12b, and S13b. Additionally, when the piezo-transmittance sensor was subjected to pressure at different vibration frequencies, the change in light transmittance remained stable (Fig. S14).

In the actual environment, the light intensity, temperature, and humidity could change at any time. Firstly, the light transmittance change under the light intensities of 100, 200, and 400 W/m^2 was investigated, and the results revealed that the light intensity had a negligible effect on the light transmittance change (Fig. 3f, S12c, and S13c). As the temperature increased from 20 to 60 °C, the obvious variations in light transmittance are not observed (Fig. 3g, S12d, and S13d). There is also no significant difference in piezo-transmittance response at different

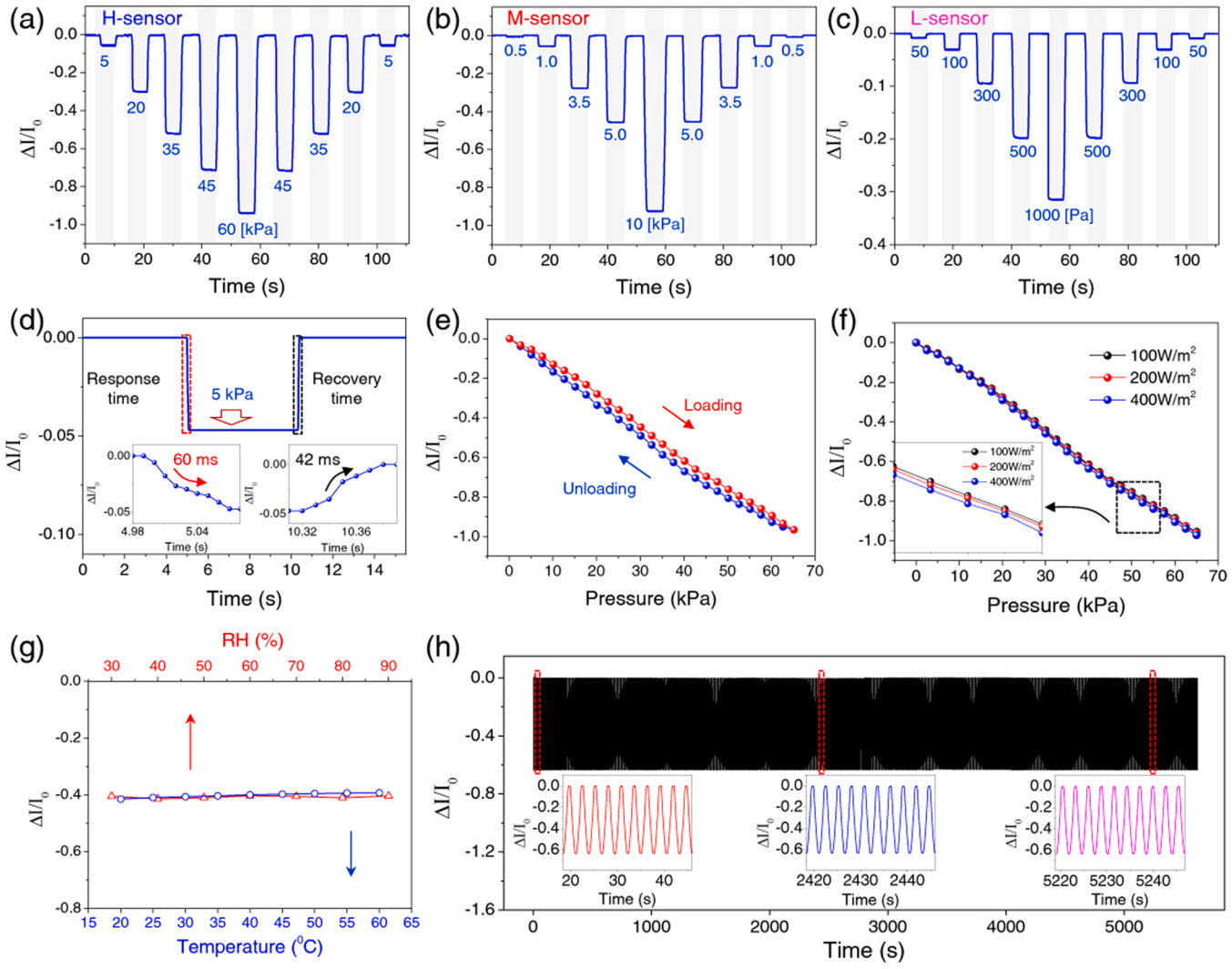

Fig. 3. Sensing performances of piezo-transmittance sensors with customizable linear pressure range. (a)–(c) The responses for the three sensors under a wide range of representative pressures. H-sensor, M-sensor, and L-sensor represent the sensor with pressure ranges of 65, 10, and 1 kPa, respectively. (d) Response time and recovery time of the H-sensor at a pressure of 5 kPa. (e) Light transmittance change of H-sensor during loading and unloading process. (f) Detection of light transmittance change of H-sensor at different light intensities of 100, 200, and 400 W/m^2. (g) Effects of temperature and humidity on the light transmittance change of H-sensor. (h) Stability and reliability of the H-sensor over 2000 loading/unloading cycles at a pressure of 40 kPa.

humidity levels ranging from 30 % to 90 % (Fig. 3g, S12d, and S13d). Long-term stability and reliability of three customized sensors were evaluated after 2000 loading/unloading cycles. The response shift and structural change cannot be detected (Fig. 3h, S12e, and S13e), demonstrating excellent repeatability. These results mean that the piezo-transmittance sensor can operate for sustained periods with different light sources in various temperature and humidity environments, thereby providing an opportunity for developing an all-weather self-powered sensing system.

2.4. *Demonstration of self-powered piezo-transmittance sensor in air flow detection*

Considering the superior performance of the pressure sensor, we further presented its applicability in various actual scenarios using solar cells and piezo-transmittance structures. Fig. S15a displays the comparison of pressure-sensing response of the H-sensor when solar cell and photodiode are respectively used as photodetectors, and the results demonstrate that their responses are almost identical. Further analysis indicates that the light transmittance of the sensor decreases with the increasing pressure, thus the theoretical minimum value of $\Delta I/I_0$ is -1 because the light can be completely blocked by the opaque tilted structures under the relatively large pressure. Moreover, a pressure sensor with a particular design has a fixed sensing range, and hence the same sensitivity can be obtained when solar cell and photodiode are respectively used as photodetectors. In addition, the rapid response (44 ms) and recovery (50 ms) are also realized using the solar cell (Fig. S15b), and the response shift and structural change cannot be detected after 1000 loading/unloading cycles (Fig. S15c), demonstrating an excellent stability and durability.

As one practical application, a self-powered wireless breathing monitoring system, which comprised a transparent mask, a piezo-transmittance sensor, two flexible solar cells (sensing solar cell and reference solar cell), an op-amp circuit, an Arduino device (Nano33 IoT), and home-made phone app, was successfully developed (Fig. 4a and 4b). The piezo-transmittance sensor was mounted on the light-sensitive area of sensing solar cell, and then attached inside the transparent mask along with the reference solar cell. In this sensing system, ambient light was used as the light source. The air flow generated during the breathing can deform the opaque tilted structures, which results in a change in the light transmittance of sensing solar cell. The output signals of sensing solar cells were processed by Arduino device and the breathing signals were transmitted to mobile device using BLE 4.0 communication protocol. Reference solar cell was applied to compensate and calibrate the response of piezo-transmittance sensor under different light intensities. The initial light transmittance value of sensing solar cell can be calculated according to the linear relationship between sensing and reference solar cells (Fig. S16).

Fig. 4c plots the current responses of sensing and reference solar cell under different light intensities. When the transparent mask was partially blocked by the hand, the output current values of both the sensing and reference solar cell decreased. After the calibration using the relationship between sensing and reference solar cell (Fig. S16), the relative light transmittance change of piezo-transmittance sensor at same breathing condition almost remained constant under different light intensities (Fig. 4c and Supporting Video 1), demonstrating the feasibility of the self-powered wireless breath monitoring system. Fig. 4d displays the current responses and corresponding relative light transmittance change under various breathing conditions. The breathing conditions including normal breath, tiny breath, hold, and fast breath

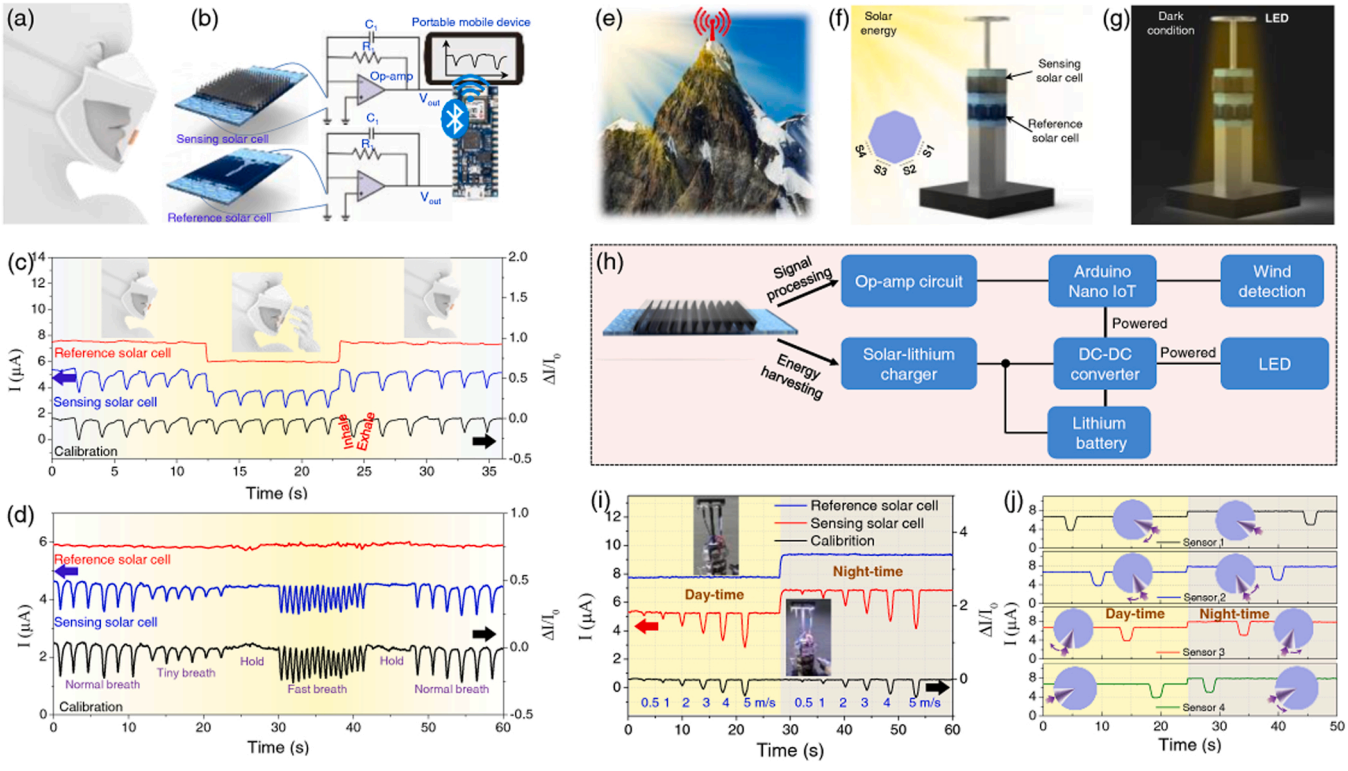

Fig. 4. Applications of the pressure sensors in air flow detection. (a) and (b) Schematic diagram depicting the mask for wireless breathing monitoring system. (c) The response of sensing and reference solar cells under different light intensities. (d) Demonstration of the sensor for monitoring different breathing conditions. (e) Schematic diagram illustrating the potential application scenarios for the detection of wind speed and direction. (f) and (g) Schematic diagram illustrating working principle under the conditions of daytime and night-time. S1, S2, S3, and S4 respectively represent four directions corresponding to sensing solar cell #1, #2, #3, and #4. (h) Schematic diagram showing the self-power circuit for simultaneous signal processing and energy harvesting. (i) Current responses and corresponding relative light transmittance change at different wind speeds (0.5, 1, 2, 3, 4, and 5 mm/s) under the conditions of daytime and night-time. (j) Current responses of sensing solar cell at different wind directions under daytime and night-time conditions.

can be clearly recognized. The real-time monitoring results obtained under different breathing conditions using a phone app are shown in Supporting Video 2.

Supplementary material related to this article can be found online at doi:10.1016/j.nanoen.2023.108299.

Supplementary material related to this article can be found online at doi:10.1016/j.nanoen.2023.108299.

The potential application of the piezo-transmittance sensor in an all-weather wind detection system at a remote site, such as mountain top (Fig. 4e), was demonstrated. Four sensing solar cells and four reference solar cells were attached to a pole in different directions, and a circular light-emitting diode (LED) array was installed at the top of the pole (Fig. 4f). During the daytime, the ambient light was utilized as light source (Fig. 4f), and the LED array provided a light source at night-time (Fig. 4g). Fig. 4h illustrates a self-powered circuit that simultaneously integrates signal processing and energy harvesting. Specifically, solar energy was harvested from solar cells for charging the lithium battery during the daytime, and then the battery provided a power supply for Arduino device and LED array through DC-DC converter at night-time.

Fig. 4i shows the current responses of sensing and reference solar cells at different wind speeds during the daytime and night-time. As the wind speed increased from 0.5 to 5 m/s, the current change of sensing solar cell gradually increased under both daytime and night-time conditions, and relative change remained stable at any wind speed. As air gun with a wind speed of 4 mm/s continuously rotated from S1 to S4 at daytime and then continuously rotated from S4 to S1 at night-time, the abrupt current signals appeared on the sensing solar cells corresponding to different directions in sequence (Fig. 4j and Supporting Video 3). Therefore, the proposed piezo-transmittance sensor can be utilized to detect wind speed and direction in both the daytime and night-time.

Supplementary material related to this article can be found online at doi:10.1016/j.nanoen.2023.108299.

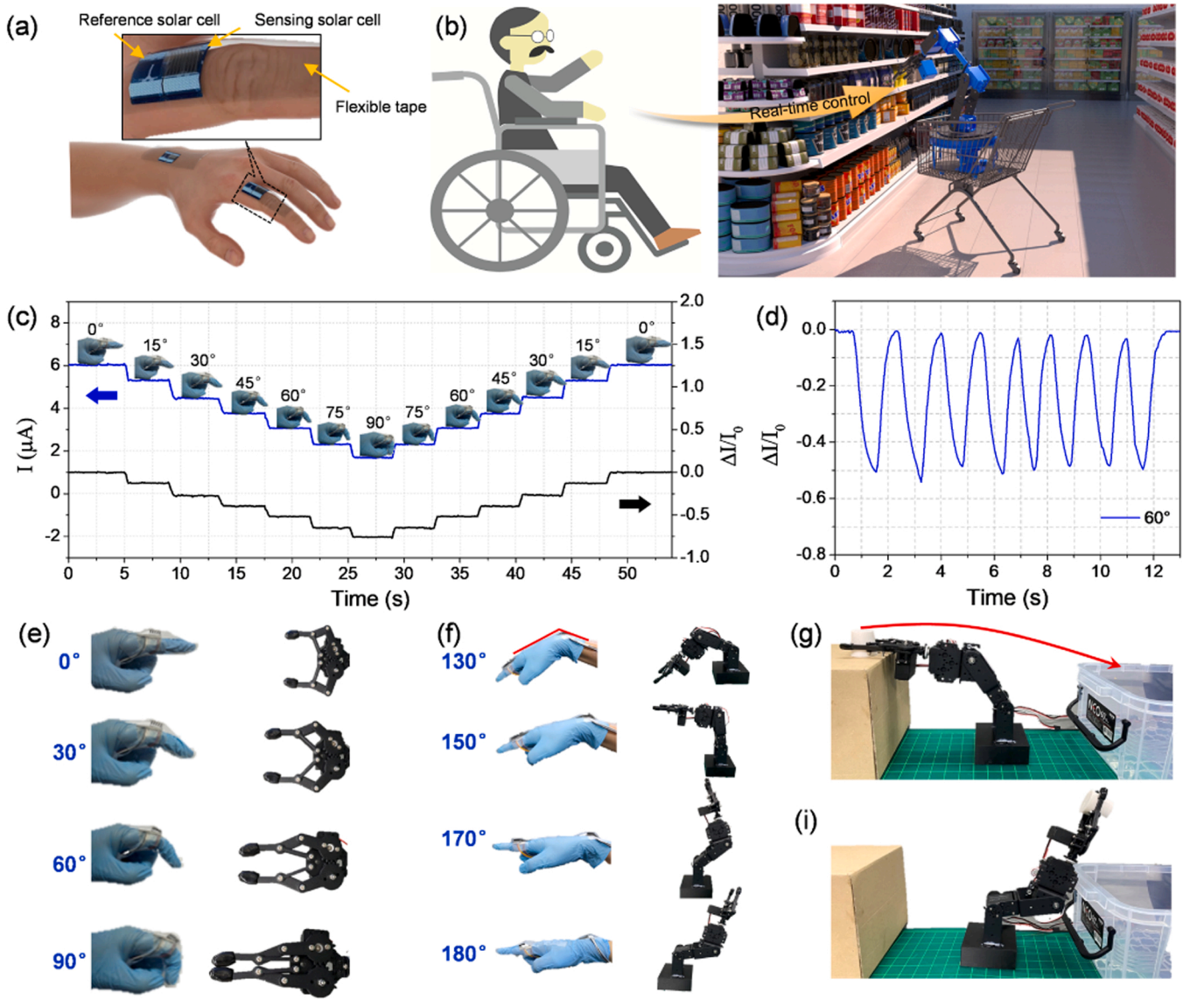

Fig. 5. Applications of the piezo-transmittance sensors in real-time control of robot gripper. (a) Schematic diagram illustrating finger and wrist bending sensor based on proposed piezo-transmittance sensor. (b) Schematic diagram depicting the potential application scenarios in the supermarket for teleoperated robotic gripper control. (c) Light transmittance response of finger bending sensor under different bending angle (0°, 15°, 30°, 45°, 60°, 75°, and 90°). (e) Light transmittance change responses of the finger bending sensor at the same bending angle (f) Photographic images of controlling the robot gripper using the sensor by bending detection of a human finger. (g) Photographic images of controlling the robot gripper movement using the sensor by bending detection of a human wrist. (h) and (i) Photographic images of teleoperated grasping process using the piezo-transmittance sensor by bending detection of finger and wrist.

2.5. Demonstration of piezo-transmittance sensor in real-time control of robot gripper

Real-time teleoperation is an effective means of manipulating a robot in an unstructured environment, which intuitively and rapidly addresses certain cases based on the human recognition [38]. We used a finger and wrist bending sensor (Fig. 5a) to demonstrate the potential application of the piezo-transmittance sensor in real-time control of robot gripper (Fig. 5b). The piezo-transmittance sensor was attached on the light-sensitive area of sensing solar cell, and a stretchable transparent tape was covered on the top surface of the sensor. When the wrist and finger were flexed, the tape compressed the tilted structures in the vertical direction, which decreased the light transmittance. Fig. 5c and S17 plot the light transmittance response of finger bending sensor at different bending angles. The sensor response gradually increased with the increasing bending angle and presented an excellent reversibility with a decrease in the bending angle. Fig. 5d further demonstrated a good stability and rapid response at the bending angle of 60°. Fig. 5e, f, and S18 further display the photographs of controlling the robot movement using the sensor by bending the finger and wrist. Therefore, the robot gripper movement can be controlled in real-time by changing the bending angle of the finger and wrist. Fig. 5g, i, and Supporting Video 4 demonstrate the control of the robot gripper movement by bending finger and wrist, thereby realizing transport of target object.

Supplementary material related to this article can be found online at doi:10.1016/j.nanoen.2023.108299.

In addition, the proposed pressure sensors can perform for both inward and outward bending conditions, and can distinguish the output signals under these two opposite conditions, as shown in Fig. S19. Specifically, a pre-load can be applied when the pressure sensor is attached to the wrist through flexible tape, and the output current of solar cell is denoted as I_0. When the wrist performs an inward bending, the light transmittance decreases because of the further deformation of the opaque tilted structures, thus output current signals of solar cells would be lower than I_0. When the wrist performs an outward bending, the pre-load is gradually released. Correspondingly, the deformed tilted structures would be gradually restored to their original state (i.e., non-compressed state), thus light transmittance of pressure sensors would increase. At this moment, the output current signals of solar cells would be higher than I_0.

3. Conclusions

The present study proposed a self-powered pressure sensor with excellent designability and customizability based on the piezo-transmittance of opaque tilted structures. Light transmittance decreases with the increasing pressure because of the deformation of opaque tilted structures. By rationally designing compressive modulus and structural parameters and optimizing cross-sectional architectures of tilted structures, the piezo-transmittance sensors with different linear pressure ranges and sensitivities could be successfully realized. The performance characterization for the customized piezo-transmittance sensors demonstrated stable, fast, and repeatable response, and their performances were hardly affected by the light intensity, temperature, and humidity. Finally, the applications of the piezo-transmittance sensor for a self-powered wireless breathing monitoring system that integrated a flexible solar cell and BLE, an all-weather wind detection system with simultaneous signal processing and energy harvesting, and a real-time teleoperated control system for robotic grasping were demonstrated. We believe that the proposed self-powered piezo-transmittance sensors with customized performances to accommodate diverse application requirements could be effectively applied in the various fields such as human-machine interface, wearable electronics, and all-weather environmental sensing systems in remote sites.

4. Experimental section

4.1. Fabrication of pressure sensor based on the piezo-transmittance of opaque tilted structures

The fabrication process of the proposed piezo-transmittance sensor is illustrated in Fig. S1. First, rectangular-parallelepiped-shaped master molds with sunken tilted array structures were fabricated using a FDM 3D printer (Ulitmaker3, USA) (Step I). Polylactic acid (PLA) was selected as printing material, and it was extruded from a 0.25-mm printing nozzle at a temperature of 210 °C. Then, the commercial elastomer base including PDMS (Sylgard 184, Dow Corning Corporation, USA) and Ecoflex (Ecoflex® Shore hardness 00–30 and 00–20, Smooth-On, Inc., USA), corresponding curing agents, and black pigment were mixed in a specified weight ratio using a planetary mixer (KK-V350W, KURABO, Japan), and the prepared mixtures were poured into the 3D printed molds (Step II). Following that, the elastomer-filled molds were placed in a vacuum chamber for 30 min to remove the bubbles. Subsequently, elastomers located in unstructured area were wiped using a wiper (Step III), and then the molds were placed in an oven to obtain semi-cured elastomers. For PDMS, the curing temperature and time were fixed at 60 °C and 20 min, respectively. For Ecoflex, the curing temperature and time were set as 40 °C and 1 min, respectively. Furthermore, transparent PDMS with a 10:1 mass ratio of base to cross-linker was poured onto the semi-cured elastomer-filled molds (Step IV). The molds were cured again in an oven for 6 h at a temperature of 60 °C, and then peeled off from the molds (Step V). Finally, structured PDMS was placed on the flat semi-cured elastomers, which were prepared by curing the PDMS with a 10:1 mass ratio of base to cross-linker for 20 min at 60 °C, and then cured at 60 °C for 6 h to form a piezo-transmittance sensor featuring a sandwich structure.

4.2. FEA simulation for piezo-transmittance sensor

The light transmittance change of pressure sensors was simulated using solid mechanics and geometrical optics modules of COMSOL Multiphysics 5.6. The dimensions of the simulation model were constructed based on the actual experimental apparatus. For Solid mechanics module, a rigid domain with a thickness of 500 μm was set at the top surface of piezo-transmittance sensor, and the bottom surface of the sensor was set as fixed constraint. The potential contact surfaces, that is, the bottom surface of top elastomer substrate, opaque tilted structures, and the top surface of bottom elastomer substrate, were set as contact pairs. A boundary load was applied perpendicularly to the sensor. For geometrical optics module, tilted structures were set as “disappear”, which can be considered that light cannot pass through these areas. The top and bottom elastomer substrates were set as “pass through” to guarantee the light to transmit from the piezo-transmittance sensor. The detection area was set as “freeze” to calculate the transmitted light from the sensor at a specified pressure.

4.3. Sensor performance characterization

An Arduino Uno with an Op-amp circuit was applied to test the performance of piezo-transmittance sensor. The Op-amp circuit included an operational amplifier (MCP6004, MICROCHIP, USA), a 300 K Ohm resistor, a 100 *nF* capacitor, and a photodiode (PD; TEMD6010FX01, Vishay, Inc., USA). Light-emitting diodes (LEDs; LS-SF5050-UE3-C, Zhejiang Guyue Longshan Electronic Technology Development Co., China) were used as light source, and the LEDs and PD were vertically aligned and mounted. A high-precision universal testing machine (AGS-X, SHIMADZU, Japan) was applied to compress the sensor at a constant speed. The cross-sectional topographies of the opaque tilted structures were detected using a charge-coupled device (CCD) camera.

4.4. Self-powered wireless monitoring system for breath detection

The wireless monitoring system composed of an Arduino board (Nano 33 IOT), two Op-amp circuits, two flexible solar cells (Powerfilm, Inc., USA) with dimensions of 12 mm × 24 mm, and a phone app designed by MIT App Inventor (App Inventor 2, Google, USA). The ambient light was used as a light source. The piezo-transmittance sensor was attached on the light-sensitive area of one solar cell, which was called as a sensing solar cell, and another one was regarded as a reference solar cell to calibrate the sensor response at different light intensities.

4.5. Self-powered monitoring system for wind speed and direction detection

Four sensing solar cells with the same piezo-transmittance sensor and four reference solar cells were mounted on the 3D printed pole at four different directions. A ring-type LED array with a tunable light intensity was installed on top of the pole. The output current signals of solar cells were also converted into voltage signals through the Op-amp circuit explained above. The four sensing solar cells were also installed in series and connected a solar-cell-lithium-battery charging integrated circuit (TP4056) to charge the lithium battery. A DC-DC converter was connected to the battery to convert the voltage from 3.7 V to 3.3 V and powered the Arduino device. The four reference solar cells were also installed in series to charge the battery using the same solar-cell-lithium-battery charging circuit, and a DC-DC converter was connected to the battery to convert the voltage from 3.7 V to 5.0 V for powering the LED array in case an external light source is needed in the dark condition. The wind speed was measured using a commercial anemometer (Testo, 450i, Germany).

4.6. Real-time teleoperation grasping by finger and wrist motion detection

Four flexible solar cells (two sensing solar cells with two piezo-transmittance sensors and two reference solar cells) were respectively attached to the finger and wrist using a flexible adhesive. A transparent tape was attached over the piezo-transmittance sensor. The output currents of solar cells were converted into voltage signals using an Arduino board (Nano 33 IOT) and an Op-amp circuit. The robot gripper and wrist motor were controlled by Arduino digital control pin, and the two motors were powered by lithium batteries (7.4 V).

CRediT authorship contribution statement

Lei Wu: Investigation, Data curation, Methodology, Writing – original draft. **Junseong Ahn:** Conceptualization, Formal analysis. **Jungrak Choi:** Methodology. **Jimin Gu:** Methodology. **Xuan Li:** Conceptualization. **Osman Gul:** Validation. **Zhi-Jun Zhao:** Methodology. **Linmao Qian:** Supervision. **Bingjun Yu:** Supervision, Writing – review & editing. **Inkyu Park:** Supervision, Conceptualization, Methodology, Writing – review & editing.

Declaration of Competing Interest

The authors declare that they have no known competing financial interests or personal relationships that could have appeared to influence the work reported in this paper.

Data availability

Data will be made available on request.

Acknowledgments

This work was supported by National Research Foundation of Korea (NRF) grant funded by the Korean government (MSIT) (No. 2021R1A2C3008742) and National Natural Science Foundation of China (52175549). Lei Wu is supported by Cultivation Program for the Excellent Doctoral Dissertation of Southwest Jiaotong University (2020YBPY04) and China Scholarship Council (202107000083).

Appendix A. Supporting information

Supplementary data associated with this article can be found in the online version at doi:10.1016/j.nanoen.2023.108299.

References

[1] X. Shi, J.J. Luo, J.Z. Luo, X.J. Li, K. Han, D. Li, X. Cao, Z.L. Wang, Flexible wood-based triboelectric self-powered smart home system, ACS Nano 16 (2022) 3341–3350.
[2] D. Liu, B.D. Chen, J. An, C.Y. Li, G.X. Liu, J.J. Shao, W. Tang, C. Zhang, Z.L. Wang, Wind-driven self-powered wireless environmental sensors for internet of things at long distance, Nano Energy 73 (2020), 104819.
[3] L.Q. Xu, W.P. Xuan, J.K. Chen, C. Zhang, Y.Z. Tang, X.W. Huang, We.J. Li, H. Jin, S. R. Dong, W.L. Yin, Y.Q. Fu, J.K. Luo, Fully self-powered instantaneous wireless humidity sensing system based on triboelectric nanogenerator, Nano Energy 83 (2021), 105814.
[4] Y. Huang, X.Y. Fan, S.C. Chen, N. Zhao, Emerging technologies of flexible pressure sensors: materials, modeling, devices, and manufacturing, Adv. Funct. Mater. 29 (2019), 1808509.
[5] J. Ahn, J.-S. Kim, Y. Jeong, S. Hwang, H. Yoo, Y. Jeong, J. Gu, M. Mahato, J. Ko, S. Jeon, J.-H. Ha, H.-S. Seo, J. Choi, M. Kang, C. Han, Y. Cho, C.H. Lee, J.-H. Jeong, I.-K. Oh, I. Park, All-recyclable triboelectric nanogenerator for sustainable ocean monitoring systems, Adv. Energy Mater. 12 (2022), 2201341.
[6] G.S. Hu, Z.R. Yi, L.J. Lu, Y. Huang, Y.Q. Zhai, J.Q. Liu, B. Yang, Self-powered 5G NB-IoT system for remote monitoring applications, Nano Energy 87 (2021), 106140.
[7] A. Ahmed, Z. Saadatnia, I. Hassan, Y.L. Zi, Y. Xi, X. He, J. Zu, Z.L. Wang, Self-powered wireless sensor node enabled by a duck-shaped triboelectric nanogenerator for harvesting water wave energy, Adv. Energy Mater. 7 (2017), 1601705.
[8] C.M. Jiang, X.J. Li, S.W.M. Lian, Y.B. Ying, J.S. Ho, J.F. Ping, Wireless technologies for energy harvesting and transmission for ambient self-powered systems, ACS Nano 15 (2021) 9328–9354.
[9] Z.X. Wang, Y.H. Wu, W.B. Jiang, Q.Y. Liu, X.B. Wang, J.W. Zhang, Z.Y. Zhou, H. W. Zheng, Z.F. Wang, Z.L. Wang, A universal power management strategy based on novel sound-driven triboelectric nanogenerator and its fully self-powered wireless system applications, Adv. Funct. Mater. 31 (2021), 2103081.
[10] M.L. Zhu, Z.R. Yi, B. Yang, C. Lee, Making use of nanoenergy from human–nanogenerator and self-powered sensor enabled sustainable wireless IoT sensory systems, Nano Today 36 (2021), 101016.
[11] Y.X. Xiong, Y.K. Shen, L. Tian, Y.G. Hu, P.L. Zhu, R. Sun, C.P. Wong, A flexible, ultra-highly sensitive and stable capacitive pressure sensor with convex microarrays for motion and health monitoring, Nano Energy 70 (2020), 104436.
[12] G.J. Zhu, P.G. Ren, J. Wang, Q. Duan, F. Ren, W.M. Xia, D.X. Yan, A highly sensitive and broad-range pressure sensor based on polyurethane mesodome arrays embedded with silver nanowires, ACS Appl. Mater. Interfaces 12 (2020) 19988–19999.
[13] Y. Guo, Z.Y. Guo, M.J. Zhong, P.B. Wan, W.X. Zhang, L.Q. Zhang, A flexible wearable pressure sensor with bioinspired microcrack and interlocking for full-range human-machine interfacing, Small 14 (2018), 1803018.
[14] Q.X. Liu, Z.G. Liu, C.G. Li, K.W. Xie, P. Zhu, B.Q. Shao, J.M. Zhang, J.L. Yang, J. Zhang, Q. Wang, C.F. Guo, Highly transparent and flexible iontronic pressure sensors based on an opaque to transparent transition, Adv. Sci. 7 (2020), 2000348.
[15] L.X. He, C.G. Zhang, B.F. Zhang, O. Yang, W. Yuan, L.L. Zhou, Z.H. Zhao, Z.Y. Wu, J. Wang, Z.L. Wang, A. Dual-Mode, Triboelectric nanogenerator for wind energy harvesting and self-powered wind speed monitoring, ACS Nano 16 (2022) 6244–6254.
[16] Y.P. Zang, F.J. Zhang, C.A. Di, D.B. Zhu, Advances of flexible pressure sensors toward artificial intelligence and health care applications, Mater. Horiz. 2 (2015) 140–156.
[17] F.L. He, X.Y. You, W.G. Wang, T. Bai, G.F. Xue, M.D. Ye, Recent progress in flexible microstructural pressure sensors toward human–machine interaction and healthcare applications, Small Methods 5 (2021), 2001041.
[18] J. Ahn, Z.-J. Zhao, J. Choi, Y. Jeong, S. Hwang, J. Ko, J. Gu, S. Jeon, J. Park, M. Kang, D. Orbe, I. Cho, H. Kang, M. Bok, J.-H. Jeong, I. Park, Morphology-controllable wrinkled hierarchical structure and its application to superhydrophobic triboelectric nanogenerator, Nano Energy 85 (2021) 105978.
[19] Y.L. Wang, W. Zhu, Y. Deng, B. Fu, P.C. Zhu, Y.D. Yu, J. Li, J.J. Guo, Self-powered wearable pressure sensing system for continuous healthcare monitoring enabled by flexible thin-film thermoelectric generator, Nano Energy 73 (2020), 104773.
[20] Q.J. Sun, X.H. Zhao, C.C. Yeung, Q. Tian, K.W. Kong, W. Wu, S. Venkatesh, W.J. Li, V.A.L. Roy, Bioinspired, self-powered, and highly sensitive electronic skin for sensing static and dynamic pressures, ACS Appl. Mater. Interfaces 12 (2020) 37239–37247.

[21] J. Gu, J. Ahn, J. Jung, S. Cho, J. Choi, Y. Jeong, J. Park, S. Hwang, I. Cho, J. Ko, J. H. Ha, Z.J. Zhao, S. Jeon, S. Ryu, J.H. Jeong, I. Park, Self-powered strain sensor based on the piezo-transmittance of a mechanical metamaterial, Nano Energy 89 (2021), 106447.
[22] J. Gu, D. Kwon, J. Ahn, I. Park, Wearable strain sensors using light transmittance change of carbon nanotube-embedded elastomers with microcracks, ACS Appl. Mater. Interfaces 12 (2020) 10908–10917.
[23] J. Choi, D. Kwon, B. Kim, K. Kang, J. Gu, J. Jo, K. Na, J. Ahn, D. Orbe, K. Kim, J. Park, J. Shim, J.Y. Lee, I. Park, Wearable self-powered pressure sensor by integration of piezo-transmittance microporous elastomer with organic solar cell, Nano Energy 74 (2020), 104749.
[24] X. Wang, M.T. Li, D. Wang, H. Zhang, R.M. Duan, D.F. Zhang, B. Song, B. Dong, Low-cost, robust pressure-responsive smart windows with dynamic switchable transmittance, ACS Appl. Mater. Interfaces 12 (2020) 15695–15702.
[25] Y. Lee, J. Park, S. Cho, Y.E. Shin, H. Lee, J. Kim, J. Myoung, S. Cho, S. Kang, C. Baig, H. Ko, Flexible ferroelectric sensors with ultrahigh pressure sensitivity and linear response over exceptionally broad pressure range, ACS Nano 12 (2018) 4045–4054.
[26] M. Amjadi, K.U. Kyung, I. Park, M. Sitti, Stretchable, skin-mountable, and wearable strain sensors and their potential applications: a review, Adv. Funct. Mater. 26 (2016) 1678–1698.
[27] S.R.A. Ruth, Z.N. Bao, Designing tunable capacitive pressure sensors based on material properties and microstructure geometry, ACS Appl. Mater. Interfaces 12 (2020) 58301–58316.
[28] J.H. Pu, X. Zhao, X.J. Zha, W.D. Li, K. Ke, R.Y. Bao, Z.Y. Liu, M.B. Yang, W. Yang, A strain localization directed crack control strategy for designing MXene-based customizable sensitivity and sensing range strain sensors for full-range human motion monitoring, Nano Energy 74 (2020), 104814.
[29] Y. Yang, X.J. Hou, W.P. Geng, J.L. Mu, L. Zhang, X.D. Wang, J. He, J.J. Xiong, X. J. Chou, Human movement monitoring and behavior recognition for intelligent sports using customizable and flexible triboelectric nanogenerator, Sci. China Technol. Sci. 65 (2022) 826–836.
[30] Y. Wang, Y. Xia, P. Xiang, Y.Y. Dai, Y. Gao, H. Xu, J.A. Yu, G.H. Gao, K.X. Chen, Protein-assisted freeze-tolerant hydrogel with switchable performance toward customizable flexible sensor, Chem. Eng. J. 428 (2022), 131171.
[31] M.-H. Seo, K. Kang, J.-Y. Yoo, J. Park, J.-S. Lee, I. Cho, B.-J. Kim, Y. Jeong, J.-Y. Lee, B. Kim, J. Rho, J.-B. Yoon, I. Park, Chemo-mechanically operating palladium-polymer nanograting film for a self-powered H_2 gas sensor, ACS Nano 14 (2020) 16813–16822.
[32] Z. Xu, D. Wu, Z. Chen, Z. Wang, C. Cao, X. Shao, G. Zhou, S. Zhang, L. Wang, D. Sun, A flexible pressure sensor with highly customizable sensitivity and linearity via positive design of microhierarchical structures with a hyperelastic model, Microsyst. Nanoeng. 9 (2023) 5.
[33] Y. Luo, J. Shao, S. Chen, X. Chen, H. Tian, X. Li, L. Wang, D. Wang, B. Lu, Flexible capacitive pressure sensor enhanced by tilted micropillar arrays, ACS Appl. Mater. Interfaces 11 (2019) 17796–17803.
[34] J. Woo, H. Lee, C. Yi, J. Lee, C. Won, S. Oh, J. Jekal, C. Kwon, S. Lee, J. Song, B. Choi, K.-I. Jang, T. Lee, Ultrastretchable Helical Conductive Fibers Using Percolated Ag Nanoparticle Networks Encapsulated by Elastic Polymers with High Durability in Omnidirectional Deformations for Wearable Electronics, Adv. Funct. Mater. 30 (2020) 1910026.
[35] Y.J. Gagnon, C.B. Roth, Local glass transition temperature $T_g(z)$ within polystyrene is strongly impacted by the modulus of the neighboring PDMS domain, ACS Macro Lett. 9 (2020) 1625–1631.
[36] P. Lu, L. Wang, P. Zhu, J. Huang, Y.J. Wang, N.N. Bai, Y. Wang, G. Li, J.L. Yang, K. W. Xie, J.M. Zhang, B. Yu, Y. Dai, C.F. Guo, Iontronic pressure sensor with high sensitivity and linear response over a wide pressure range based on soft micropillared electrodes, Sci. Bull. 66 (2021) 1091–1100.
[37] C. Ma, D. Xu, W.F. Liu, T.Y. Dong, S.T. Li, Mould-free skin-inspired robust and sensitive flexible pressure sensors with hierarchical microstructures, IEEE Electr. Device Lett. 42 (2021) 1536.
[38] C. Meeker, M. Haas-Heger, M. Ciocarlie, A continuous teleoperation subspace with empirical and algorithmic mapping algorithms for nonanthropomorphic hands, IEEE Trans. Autom. Sci. Eng. 19 (2020) 373–386.

Lei Wu is a Ph.D. candidate at Southwest Jiaotong University. He received his Bachelor degree in Mechanical design, manufacturing and automation in 2017 from Southwest Petroleum University, China. His current research interest is focused on chemical & physics sensors based on functional micro/nanostructures.

Junseong Ahn is a Ph.D. candidate at the Korea Advanced Institute of Science and Technology (KAIST). He received his M.S. degree at KAIST in 2019. His current research interest is focused on micro/nano structuring, and their application to sensors/energy harvesting devices.

Jungrak Choi is a Ph.D. candidate at the Korea Advanced Institute of Science and Technology (KAIST). He received his M.S. degree at KAIST and DTU in 2018. His current research interest is focused on soft sensors and stretchable electronics for healthcare applications.

Jimin Gu is a Ph.D. candidate at the Korea Advanced Institute of Science and Technology (KAIST). She received her M.S. degree at KAIST in 2019. Her current research interest is focused on soft sensors and stretchable electronics for biomedical and healthcare applications.

Xuan Li is a master candidate at the Korea Advanced Institute of Science and Technology (KAIST). She received her Bachelor degree in environmental engineering in 2020 from Shandong University, China. Her research interest is focused on self-powered sensors.

Osman Gul is a Ph.D. candidate at the Korea Advanced Institute of Science and Technology (KAIST). He received his M.S. degree at KAIST in 2022. His current research interest is soft sensors for healthcare applications.

Zhi-Jun Zhao received his Ph.D. degree at Pusan National University in 2018. He is associate Professor of Institute of Smart City and Intelligent Transportation at Southwest Jiaotong University. His research interests are micro-nanofabrication, optical devices, nanomaterial-based sensors, and flexible & wearable electronics.

Linmao Qian received his B.S. (1994) and Ph.D. (2000) in Mechanical Engineering from Tsinghua University. He joined the faculty at Southwest Jiaotong University in 2002. He is dean and full professor of Mechanical Engineering at Southwest Jiaotong University. His research interest includes nanotribology and ultra-precision manufacturing.

Bingjun Yu received his Ph.D. in Mechanical Engineering from Southwest Jiaotong University in 2012. From Sep. 2015 to Sep. 2016, he did research on nanofabrication at University College London. He is Professor of Mechanical Engineering at Southwest Jiaotong University. His research interest includes nanofabrication, nanomanipulation and nanotribology.

Inkyu Park received his B.S., M.S., and Ph.D. from KAIST (1998), UIUC (2003), and UC Berkeley (2007), respectively, all in mechanical engineering. He has been with the Department of Mechanical Engineering at KAIST since 2009 as a faculty member and is currently a KAIST Chair Professor. His research interests include nanofabrication, smart sensors, nanomaterial-based sensors, and flexible & wearable electronics.